The HKU Scholars Hub   The University of Hong Kong   香港大學學術庫

Title	**Diffraction-limited 3 μ m spectroscopy of IRAS 04296+3429 and IRAS 05341+0852: Spatial extent of hydrocarbon dust emission and dust evolutionary sequence**
Author(s)	**Goto, M; Kwok, S; Takami, H; Hayashi, M; Gaessler, W; Hayano, Y; Iye, M; Kamata, Y; Kanzawa, T; Kobayashi, N; Minowa, Y; Nedachi, K; Oya, S; Pyo, TS; SaintJacques, D; Takato, N; Terada, H; Henning, Th**
Citation	**The Astrophysical Journal, 2007, v. 662 n. 1, p. 389-394**
Issued Date	**2007**
URL	**http://hdl.handle.net/10722/179706**
Rights	**The Astrophysical Journal. Copyright © University of Chicago Press.**

DIFFRACTION-LIMITED 3 μm SPECTROSCOPY OF IRAS 04296+3429 AND IRAS 05341+0852: SPATIAL EXTENT OF HYDROCARBON DUST EMISSION AND DUST EVOLUTIONARY SEQUENCE[1]

Miwa Goto,[2,3] Sun Kwok,[4] Hideki Takami,[5] Masa Hayashi,[5] W. Gaessler,[2] Yutaka Hayano,[5] Masanori Iye,[6] Yukiko Kamata,[6] Tomio Kanzawa,[5] Naoto Kobayashi,[7] Yosuke Minowa,[7] Ko Nedachi,[5] Shin Oya,[5] T.-S. Pyo,[5] D. Saint-Jacques,[8] Naruhisa Takato,[5] Hiroshi Terada,[5] and Th. Henning[2]

ABSTRACT

We present 3 μm spectroscopy of the carbon-rich protoplanetary nebulae IRAS 04296+3429 and IRAS 05341+0852, conducted with the adaptive optics system at the Subaru Telescope. We utilize the nearly diffraction-limited spectroscopy to probe the spatial extent of the hydrocarbon dust emitting zone. We find a hydrocarbon emission core extending up to 100–160 mas from the center of IRAS 04296+3429, corresponding to a physical diameter of 400–640 AU, assuming a distance of 4 kpc. However, we find that IRAS 05341+0852 is not spatially resolved with this instrumentation. The physical extent of these protoplanetary nebulae, along with the reanalyzed data of IRAS 22272+5435 published previously, suggests a correlation between the physical extent of the hydrocarbon dust emission and the spectral evolution of the aliphatic to aromatic features in these post-AGB stars. These measurements represent the first direct test of the proposed chemical synthesis route of carbonaceous dust in the circumstellar environment of evolved stars.

Subject headings: circumstellar matter — dust, extinction — infrared: ISM — ISM: evolution — stars: AGB and post-AGB — stars: individual (IRAS 04296+3429, IRAS 05341+0852, IRAS 22272+5435)

1. INTRODUCTION

The origin of carbonaceous grains observed in the interstellar medium and in the early solar system is a topic of great interest. These grains are composed of a chain or a network of carbon atoms bonded to hydrogen atoms at their periphery with physical and chemical properties intermediate between those of simple molecules and of bulk solid particles. Due to the versatility of carbon atoms in creating various hybridized bonds, these carbonaceous grains can have very complex chemical structures (Henning & Salama 1998; Ehrenfreund & Charnley 2000; Pendleton & Allamandola 2002; Henning et al. 2003).

Recent infrared spectroscopic observations from space have revealed that carbon-rich post–asymptotic giant branch (post-AGB) stars undergo rapid synthesis of hydrocarbon grains with both aromatic and aliphatic signatures. The aromatic hydrocarbon is characterized by benzene-like rings in which carbon atoms are connected to each other with conjugated double bonds, while the aliphatic hydrocarbon consists of linear chains or a network of carbon atoms connected by saturated bonds. The production and ejection of these grains may play a significant role in the chemical enrichment of the interstellar medium and the early solar system (Kwok 2004). Specifically, while carbon-rich AGB stars show either the 11.3 μm feature due to SiC or a featureless continuum due to amorphous carbon (Henning & Mutschke 2001; Clément et al. 2003), aromatic features at 3.3, 6.2, 7.7, 8.6, and 11.3 μm and aliphatic features at 3.4 and 6.9 μm begin to appear in protoplanetary nebulae (PPNs; Kwok et al. 1999). We now know that the aliphatic to aromatic transformation of the circumstellar dust from PPNs to planetary nebulae coincides with environmental changes of increasing stellar temperature, less protective dusty environment, and the outbreak of harsh UV radiation (Kwok et al. 2001). In order to test any photochemical models, we first need a good knowledge of the spatial distribution of the emitting materials. The observations of these objects in the short transition phase between AGB stars and planetary nebulae are therefore of primary importance in our understanding of the chemical synthesis of carbonaceous grains.

IRAS 04296+3429, along with IRAS 05341+0852 and IRAS 22272+5435, belongs to a small group of PPNs with extremely carbon-rich chemistry, first recognized by the presence of an unidentified 21 μm emission feature in their *IRAS* Low-Resolution Spectrometer spectra (Kwok et al. 1989, 1995). The observational properties of these sources, taken from the literature, are summarized in Table 1. This class of PPN is most exclusively characterized by prominent emission features of highly aliphatic material with broad emission at 3.4 μm alongside the common aromatic feature at 3.3 μm first detected by Geballe & van der Veen (1990) and Geballe et al. (1992), and subsequently classified in Geballe (1997). Since the hydrocarbon dust is synthesized in the circumstellar environment, if it undergoes temporal modification it will leave a record of unique spatial distribution in the circumstellar envelope. With sufficient spatial resolution, we may observe the history of dust formation as a change of hydrocarbon dust structure with distance from the central star. Such observations provide a critical test for the proposed evolutionary schemes (e.g., Kwok et al. 1999). However, PPNs are usually small in angular extent and require subarcsecond resolution to image. It is only recently that the imaging resolution in the infrared has become good enough to perform such experiments (Goto et al. 2003). In this paper, we present high angular resolution imaging spectroscopy of the distribution of circumstellar hydrocarbon dust using an adaptive optics (AO) system.

2. OBSERVATIONS

The 3 μm spectra of IRAS 04296+3429 and IRAS 05341+0852 were obtained at the Subaru Telescope atop Mauna Kea on

TABLE 1
STELLAR PROPERTIES

Star	R. A. (J2000.0)	Decl. (J2000.0)	Spectral Type	V Magnitude	L Magnitude	d (kpc)	L_* ($L_\odot$)	T_d (K)	References
IRAS 04296+3429...............	04 32 57.0	+34 36 13	G0 Ia	14.17	7.4	4.0/7.1	5300/(8000[a])	200	1, 2, 3, 4
IRAS 05341+0852...............	05 36 55.0	+08 54 08	F4 Iab	13.61	8.13	7.4	(8000[a])	210	1, 2, 5
IRAS 22272+5435...............	22 29 10.4	+54 51 07	G5 Ia	9.10	4.43	1.8	13000	202	1, 6, 7, 8

[a] The total luminosity is assumed to be $L_* = 8000\ L_\odot$ when estimating the distance to the source.

REFERENCES.—(1) Ueta et al. 2000; (2) Fujii et al. 2002; (3) Manchado et al. 1989; (4) Meixner et al. 1997; (5) Geballe & van der Veen 1990; (6) Hrivnak & Kwok 1991; (7) J. Nakashima 2006, private communication; (8) Ueta et al. 2001.

2001 December 23 with the Infrared Camera and Spectrograph (IRCS; Tokunaga et al. 1998; Kobayashi et al. 2000). An AO system was used as a front-end instrument to feed wavefront–compensated images to IRCS. The Subaru AO is a 36 element curvature-based system installed at the telescope Cassegrain port (Gaessler et al. 2002; Takami et al. 2004). It delivers diffraction-limited images at wavelengths longer than 2 μm. A medium-resolution grism was used with a 0.30″ slit to provide spectra with a resolving power of $\lambda/\Delta\lambda = 600$–800. The plate scale of the spectrograph was 58 mas pixel^{-1} along the slit. The slit was aligned to P.A. = 28° and 98° for IRAS 04296+3429, along the disk and the bipolar lobe projected on the sky (Sahai 1999). The slit was rotated to P.A. = 45° for IRAS 05341+0852, which is along the elongation of the nebula at optical wavelengths (Ueta et al. 2000). The visible central stars of IRAS 04296+3429 (1200−02336188 in the USNO-A2.0 catalog; $R = 13.7$ mag) and IRAS 05341+0852 (0975-01778353; $R = 12.7$ mag) were used as the wavefront references for the AO system. The spectrograms were recorded by wobbling the AO system's tip-tilt mirror by ±1.5″ along the slit. A G0.5 V star, HR 660 ($R = 4.5$ mag), was observed at the beginning of the observation through similar airmass to calibrate for atmospheric transmission. The mismatch in airmass between this reference and the observed objects was smaller than 0.1. In order to use HR 660 as the standard star for the point-spread function (PSF) as well, HR 660 was dimmed by neutral density filters in front of the wavefront sensor until the output counts of the avalanche photodiodes were comparable to those of the objects, so that the corrected wavefront error would be similar. The observation of IRAS 04296+3429 was completed within 1.3 hr of observing HR 660 for the first slit position at P.A. = 98°. HR 660 may not be as good a PSF standard for IRAS 05341+0852, as this was observed nearly 4 hr later. The PSF as measured with HR 660 provides an independent measurement to test the spatial extent of IRAS 04296+3429, as discussed in § 3.1. The spectroscopic flat field was made at the end of the night using a halogen lamp installed at the calibration unit in front of the instrument entrance window. The seeing was good at the beginning of the night (0.55″ at R), deteriorating toward the end of the observation (0.86″ at R). The details of the observation of IRAS 22272+5435 are presented elsewhere (Goto et al. 2003).

3. DATA ANALYSIS

3.1. Nonlinearity Correction

Data reduction begins with correcting each frame for detector nonlinearity, since even slight saturation of the detector response affects the PSF measurement required in the present study. Suppression of pixel counts at the peak of the PSF modifies the spatial profile by making it slightly flatter. Therefore, the measured spatial width is increased. Special care must be taken to take into account the pixel counts in the pedestal readout. A typical readout of an infrared detector array consists of three steps: a reset of the entire array, after which integration starts immediately; a first readout to sample the pixel counts at the beginning of the exposure; and a second readout after the desired integration time. Then the pedestal count from the first readout is subtracted, yielding the net signal. This net signal is usually monitored during observations so as not to exceed the detector linearity limit.

However, for observations in high-flux regime, such as the ones done with the AO system, the integration time can be so short that it is comparable to the detector readout time. Substantial photon flux is already accumulated in the pixel before the first readout. The pedestal counts can potentially push the second readout up into the nonlinear regime, a situation that cannot be recognized when only the net signal is monitored. The pedestal count depends on how soon the relevant pixel is read after the array reset, and therefore depends on the location of the pixel in the array. The magnitude of the nonlinearity correction, including the position-dependent pedestal count, amounts to not more than 8% in most of the observations with our setup, using a pixel readout of 0.41 s for the entire array, an integration time of 8 s, and maximum net counts restricted to values below 5000 ADU.

3.2. Spectroscopy

Following the above described nonlinearity correction, consecutive spectrograms were subtracted from each other to eliminate background sky emission. Pixel-to-pixel detector response variation was normalized by ratioing with dark-subtracted flat-field images. The extraction aperture was defined at a fixed distance from the profile centroid, and the enclosed pixel counts were summed to produce a one-dimensional spectrum. Wavelength calibration was performed by maximizing the correlation of resulting spectrum with a model atmospheric transmission curve computed by ATRAN (Lord 1992). Telluric atmospheric absorption features were removed by dividing by the spectrum of the spectroscopic standard star HR 660.

The results are shown in Figure 1 for IRAS 04296+3429 and IRAS 05341+0852, after normalization by a polynomial function fitted to the continuum emission in order to highlight the hydrocarbon emission features at 3.2–3.6 μm. The spectrum of IRAS 22272+5435 extracted from the off-center region of the nebula, originally published in Goto et al. (2003), is shown for comparison. Two parallel trends are noticeable. First, the aliphatic emission feature at 3.4 μm, specific to this class of carbon-rich PPNs, diminishes as one progresses from IRAS 05341+0852 to IRAS 04296+3429 and to IRAS 22272+5435, with respect to the aromatic emission at 3.3 μm. At the same time, the overall intensity of hydrocarbon emission above the continuum decreases.

Large-scale (>0.5″) variations of the spectral shape of the emission feature were checked for IRAS 04296+5435 and IRAS 05341+0852 in the same way as for IRAS 22272+5435, by shifting the extraction aperture from the central star (Goto et al. 2003). The flux at the off-center regions is dominated by the PSF halo of
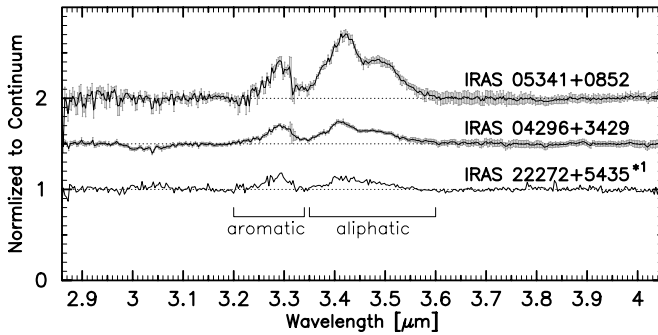
Fig. 1.—Spectra of IRAS 05341+0852 and IRAS 04296+3429 after division by a polynomial fit to the continuum. Also plotted is the spectrum of IRAS 22272+5435 from Goto et al. (2003). These three PPNs are extremely carbon-rich, with specific aliphatic emission features at 3.4 μm, along with more common aromatic emission at 3.3 μm. The intensity of the aliphatic emission relative to the aromatic feature decreases with the physical development of the nebulae. The ratio of the whole emission feature to the continuum emission exhibits the same trend. Note that the spectrum of IRAS 22272+5435 is extracted from the nebula, but in a region offset from the central star, in order to highlight the hydrocarbon emission features. The feature-to-continuum ratio is much smaller when the central star is included, which makes the trend above even stronger.

the central star, and no significant difference was observed between the spectra extracted at the central stars and those taken from the off-center regions.

3.3. Spatial Profiles

The AO system is a powerful tool, providing superb spatial resolution for imaging and spectroscopy. However, the outcome is sometimes highly variable when we work at the performance limit, being dependent on the variability of observing conditions.

The reference PSF varies according to the seeing, the brightness of the wavefront reference source, and the observing wavelength (and therefore the color of each object). This variable PSF makes the interpretation of the spatial extent of observed sources a challenge. For instance, when stellar images look larger for one source than for the other, there is no way to tell whether the source indeed has a circumstellar structure, or whether the seeing has simply become worse. This uncertainty can be eliminated if a point-source reference is observed at the same time with the same instrumental setup, and preferably in the same frame, which is often not the case.

We used spectroscopy as a means of sampling a reference PSF within frames. Spectroscopy amounts to simultaneous imaging at multiple wavelengths over hundreds of spectral elements, although the imaging is spatially one-dimensional. If certain spectral features are spatially extended, this is most sensitively detected by differentiating the spatial profile from that of the immediate continuum region. The scheme is illustrated in Figure 2. In the present observations, we have compared the cross section of the spectrogram at the hydrocarbon dust emission wavelength with the nearby continuum. The spatial profile of IRAS 04296+3429 in Figure 2 is wider at the level of the emission feature by approximately by 16% compared to the continuum wavelength. This difference in the widths of the two spectral regions is not large, but it is real; otherwise the spatial profiles at these two spectral regions would be identical, as it is the case for the comparison star HR 660 shown in the same figure.

Since spatial profiles are sparsely sampled in pixelized data, the pixel data must be interpolated in order to quantitatively parameterize the spatial profile. Empirically, we found that the observed PSF is better approximated by a Lorentzian than by a single-component Gaussian, given the high wings resulting from of the
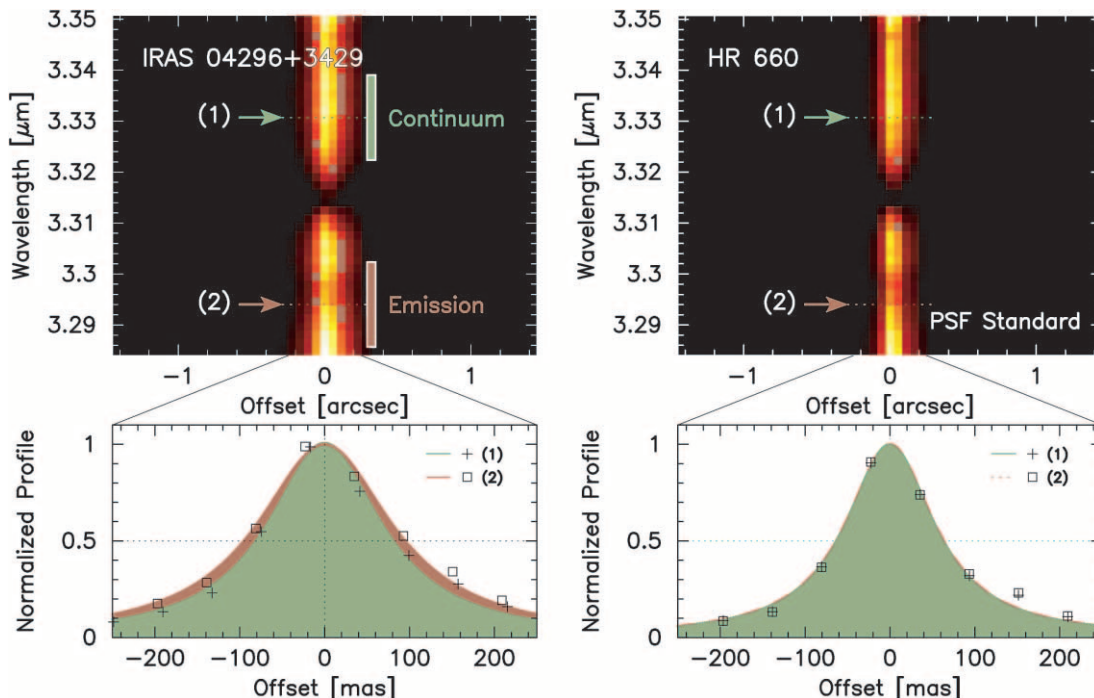

Fig. 2.—*Top left*: Close-up view of the spectrogram of IRAS 04296+3429 at 3.29–3.35 μm. The spectrogram is pair-subtracted and flat-fielded. The aromatic hydrocarbon dust produces emission at 3.3 μm, which is marked as "Emission" in the spectrogram. The 3.32–3.34 μm region, in between the 3.3 μm aromatic and the 3.4 μm aliphatic feature, is labeled as "Continuum." *Bottom left*: One-dimensional slice of the spectrogram cut along the slit at the emission wavelength (*rectangles*) and on the continuum (*plus signs*). The green and red filled curves are Lorentzian functions used to fit the pixel data at the continuum and at the emission feature, respectively. It is evident that IRAS 04296+3429 is larger at the 3.3 μm aromatic feature than at the continuum wavelength. *Right*: Same as left panels, but for the standard star HR 660. In this case, the spatial profiles of the two spectral regions are almost identical.
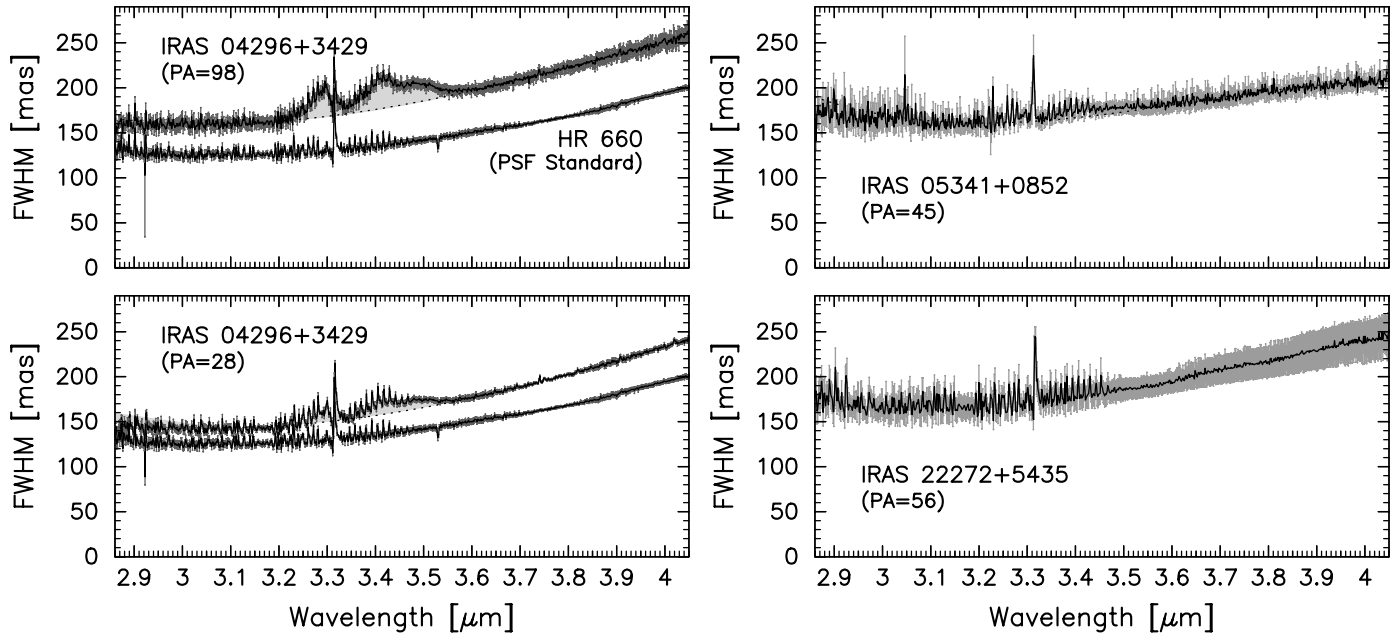
FIG. 3.—Variation of the FWHM of the sources as a function of wavelength. *Top left*: Spatial extent of IRAS 04296+3429 at P.A. = 98° along the bipolar lobe. The smooth increase in FWHM with wavelength represents the diffraction-limited behavior of a PSF. This wavelength dependence is fitted by a dotted line, and any excess above it is emphasized by light gray shading. The error bars are given by the dispersion of the FWHM in the repeated measurements (*dark gray shading*). The spatial extent of the standard star HR 660 is plotted in the same panel for comparison, as well as the polynomial fit to the continuum of the FWHM spectrum of IRAS 04296+3429, used as the PSFs in the later deconvolution. *Bottom left*: Variation of spatial extent of IRAS 04296+3429 measured at P.A. = 28° along the disk. *Top right*: Variation of spatial extent of IRAS 05341+0852 measured along P.A. = 45°. *Bottom right*: Variation of spatial extent of IRAS 22272+5435 measured along P.A. = 56°.

first ring and the seeing halo around the diffraction core (Fig. 2). The bad pixels with outlying responses were deliberately left uncorrected, because smoothing outlier pixels modifies the intrinsic spatial profile, leading to an incorrect spatial width.

The full width at half-maximum (FWHM) of the spatial profiles was derived from these fits, and was measured at each spectral element from 2.9 to 4.1 μm. The "FWHM spectrum," the variation of FWHM as a function of the wavelength, was measured separately in each frame to preserve spatial resolution. They were then combined for each source. The results are shown in Figure 3. The spatial width of IRAS 04296+3429 is clearly extended near the 3.3–3.4 μm hydrocarbon emission features, compared to its size at continuum wavelengths.

The spectroscopic data for IRAS 22272+5435, obtained by Goto et al. (2003), were reprocessed in the same manner as described here, and the resulting FWHM spectrum is shown in Figure 3 for comparison with IRAS 04296+3429 and IRAS 05341+0852.

3.4. Deconvolution

The spatial width we measured in § 3.3 is a stellar angular diameter convolved with the system PSF. In order to derive the intrinsic dimension of the emitting region, we need to deconvolve the PSF from the apparent spatial width. For this task, we assume that the observed spatial width is a simple squared sum of the intrinsic angular size and the size of the PSF at that wavelength,

$$\theta_{\rm obs}^2(\lambda) = \theta_*^2(\lambda) + \theta_{\rm PSF}^2(\lambda).$$

Obtaining the correct PSF, $\theta_{\rm PSF}(\lambda)$, is not a trivial task, since the wavelength-dependent PSF changes with AO performance at the time of observing. We calculate the intrinsic physical dimension $\theta_*(\lambda)$ in two ways, assuming different $\theta_{\rm PSF}(\lambda)$ at deconvolution.

First, we assume that the continuum emission of IRAS 04296+ 3429 is an unresolved point source. We measure only the *relative*

dimension of the hydrocarbon emitting region with respect to the continuum dust emission. The apparent diameter of IRAS 04296+ 3429 smoothly increases at longer wavelengths, except near the hydrocarbon emission features and at the spikes of heavy absorption by methane in the telluric atmosphere at 3.2–3.4 μm. A polynomial function is fit to the continuum of the FWHM spectrum, and is taken as $\theta_{\rm PSF}(\lambda)$ (Fig. 3). The large $\theta_{\rm PSF}(\lambda)$ assumed here provides a stringent lower limit for the extent of the hydrocarbon emitting zone. The apparent angular diameter of the continuum emitting region is 180 mas at 3.4 μm at P.A. = 98°, as is shown by the fit in Figure 3. On the other hand, the apparent FWHM is well above 200 mas at the hydrocarbon emission features, yielding a minimum physical diameter for the hydrocarbon emitting region of ∼100 mas (Fig. 4), corresponding to 400 AU in diameter, assuming a distance of 4 kpc for IRAS 04296+3429 (Meixner et al. 1997).

In an alternative approach, we assume that the system PSF was stable throughout the observations and simply use the apparent diameter of HR 660 as $\theta_{\rm PSF}(\lambda)$ to deconvolve the FWHM of IRAS 04296+3429. This assumption allows an *absolute* estimate of the actual physical dimension of IRAS 04296+3429. The deconvolved FWHM of IRAS 04296+3429 by this method is 160 mas at 3.4 μm. The corresponding physical dimension of the hydrocarbon core is 640 AU (P.A. = 98°) in diameter (Fig. 4).

IRAS 04296+3429 is apparently larger than HR 660 at all the wavelengths observed in the present study (Fig. 3), which may suggest that even the continuum emission is indeed extended and not a point source as we assumed in the first method. However, it is not clear which of the methods described above is better suited to this particular case, as the dust emission tops the stellar component exactly at the relevant wavelengths near 3–4 μm (Kwok 1993; Ueta et al. 2000; Fujii et al. 2002), which implies the continuum emission is still dominated by the stellar point source; although there could be a substantial contribution to the continuum
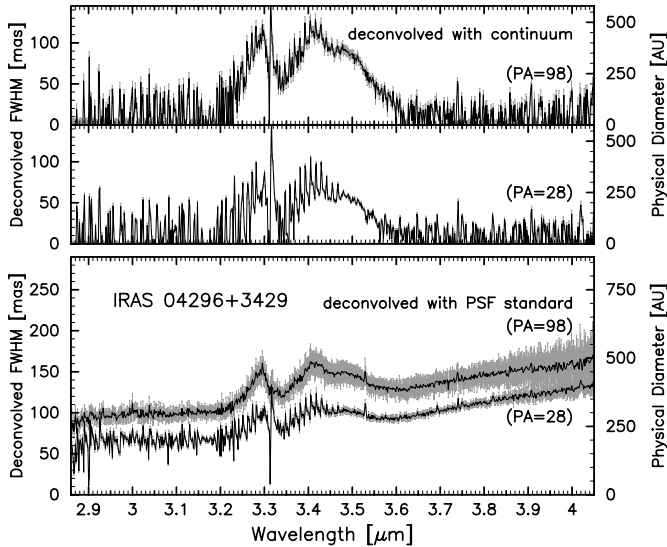
Fig. 4.— Variation of the size of the hydrocarbon emission zone as a function of wavelength after deconvolution. *Top*: FWHM spectra deconvolved with the continuum FWHM of IRAS 04296+3429 itself; assuming the continuum emission is a point source, and smoothly increases with wavelength as is in the polynomial fit shown in dotted lines in Fig. 3. *Bottom*: FWHM spectra deconvolved using the FWHM of the standard star HR 660 as the PSF. The upper trace is for measurements along P.A. = 98°, and the lower trace for P.A. = 28°. The angular scale on the left vertical axis is converted to physical size on the right vertical axis, assuming a distance of 4 kpc (Meixner et al. 1997).

emission in the 3 μm region from very small, stochastically heated grains.

4. DISCUSSION

From *Hubble Space Telescope* optical imaging, we know that IRAS 04296+3429 consists of three major components: a large spherical halo; a disk seen in the scattered light; and a bipolar lobe nearly vertical to the disk, plunging into the surrounding halo (Sahai 1999). The halo is the remnant of the circumstellar material ejected during the previous AGB phase. The bipolar lobe, delineated by its interface to the halo, is supposed to be collimated by the disk. This geometry is typical of PPNs and we assume that they were formed in the following order: the halo, the disk, and the bipolar lobes. The newly found hydrocarbon emitting region is much smaller in size than all of the above three components, and does not correspond to any of the structures previously imaged in visible light. The double-peaked spectral energy distribution observed in this object suggests that the dust shell is detached from the central star and that large-scale mass loss has ceased some time in the past (Kwok et al. 1989). However, the compact hydrocarbon dust emitting region found in this paper implies that carbon dust formation is still in progress in IRAS 04296+3429. This provides direct proof that aromatic and aliphatic hydrocarbon dust is being made in the circumstellar environment during the post-AGB phase.

Since the distribution of the hydrocarbon dust emission has been measured in three PPNs, we can use these results to determine their evolutionary status within the post-AGB evolution sequence. The wider FWHM compared to the continuum emission region is interpreted as the hydrocarbon dust being spatially extended. Its total luminosity is at least comparable to that of the continuum emission.

The hydrocarbon dust around IRAS 22272+5435 is distributed between 700 and 1500 AU from the central star (Goto et al. 2003). This is twice as large as the hydrocarbon dust core in IRAS

04296+3429. We applied the same analysis to IRAS 22272+5435 as to IRAS 04296+3429 to see if there is any extended but compact emission core in the central region of the nebula (Fig. 3). We found no excess of the FWHM at the central star, although IRAS 22272+5435 is closer to us (d = 1.8 kpc; J. Nakashima 2006, private communication; based on the formula presented in Deguchi et al. 2002),[9] indicating that the hydrocarbon dust in IRAS 22272+5435 has been cleared up and the central star can already be seen through the dust envelope.

No enhancement is observed in the width of the spatial profile at the hydrocarbon emission wavelength for IRAS 05341+0852 (Fig. 3). At first glance, the FWHM spectrum of IRAS 05341+0852 looks similar to that of IRAS 22272+5435, in which the dust emitting region has developed as much as 1.5″ in diameter. To the contrary, as we will discuss, the hydrocarbon emission in IRAS 05341+0852 is compact and unresolved. First, a crucial difference between the two sources is the lack of diffuse emission of hydrocarbon dust around IRAS 05341+0852. We checked on any possible spatial variation of the hydrocarbon emission feature in IRAS 05341+0852 with the same analysis we used for IRAS 22272+5435 in Goto et al. (2003). If positively detected, a spatial variation would provide unambiguous evidence of a physically extended hydrocarbon dust emitting zone. However, not only was such a variation not detected, but even the intensity of the emission feature relative to the continuum level is constant regardless of the distance from the central star, which is consistent with a point source and favors the interpretation that the hydrocarbon emission in IRAS 05341+0852 is unresolved. Second, we will estimate the dust emitting region of IRAS 05341+0852, assuming that the general morphology of the nebula is same with IRAS 22272+5435. The nebulosity around IRAS 22272+5435 spans 3.47″ × 3.37″ in I band (Ueta et al. 2000), and is smaller in the mid-infrared (1.3″ × 1.0″ at 8 μm; averaged from Meixner et al. 1997 and Ueta et al. 2001). The mid-infrared dimension is roughly comparable to the detached hydrocarbon emitting zone located by Goto et al. (2003). IRAS 05341+0852 appears much smaller in I band, presumably because of the greater distance to the source (1.14″ × 0.78″; Ueta et al. 2000). If we simply scale the near-infrared appearance of IRAS 05341+0852 according to the relative dimension of IRAS 22272+5435 in the mid and near-infrared, the hydrocarbon emitting region of IRAS 05341+0852 should measure 0.2″–0.4″ from the central star. If IRAS 05341+0852 has a detached hydrocarbon emitting region comparable to that of IRAS 22272+5435, it should have been spatially resolved by the present observation, even at the apparent large distance to IRAS 05341+0852.

Here we try to place an upper limit on the physical extent of the hydrocarbon dust in IRAS 05341+0852. The distance to the PPN is poorly known. We take a conservative value of d = 7.4 kpc to IRAS 05341+0852 from Fujii et al. (2002), which assumes the typical intrinsic luminosity of PPNs to be $L_* = 8000\,L_\odot$. The FWHM of IRAS 05341+0852 is averaged to 174.5 ± 8.5 mas in the range of 3.2–3.6 μm. The uncertainty sets the upper limit for the physical extent of hydrocarbon emitting zone to 54.2 mas after deconvolution, which translates to 400 AU at the distance

---

[9] The distance to IRAS 22272+5435 was updated from the 1.6 kpc previously used in Goto et al. (2003), and Ueta et al. (2001). The physical size of the nebula is scaled up accordingly. This new estimation is based on a simple comparison of the apparent luminosity of the nebula obtained from photometric data ranging from the visible to the infrared, with an assumed intrinsic luminosity of 8000 $L_\odot$, typical for a PPN. The interstellar extinction is not accounted for, which may affect the visible part of the spectral energy distribution. This distance is therefore an upper limit, yielding an upper limit for the physical extent of the hydrocarbon emitting region at IRAS 22272+5435.

quoted above. Therefore, if IRAS 05341+0852 has a dust emission core with similar spatial extent to IRAS 04296+3429 ($\sim$400 AU), it should have been detected even at that distance, although admittedly only marginally. In order to be consistent, if we use 7.1 kpc as the distance to IRAS 04296+3429, as proposed by the same authors using the same method, instead of the 4 kpc given by Meixner et al. (1997), the physical extent of the hydrocarbon emitting zone around IRAS 04296+3429 increases to $D \approx$ 1100 AU. This makes it even safer to say that the physical extent of IRAS 05341+0852 is less than that of IRAS 04296+3429, and if the former had a hydrocarbon core similar to the other one in size, it would be detectable. We therefore conclude IRAS 05341+0852 is unresolved, not because of its remote location, but because the hydrocarbon emission region is intrinsically small in size.

We now have the distribution of hydrocarbon dust in three PPNs: the emitting region in IRAS 05341+0852 is unresolved; in IRAS 04296+3429 it is concentrated but extended up to 400–640 AU in diameter; and in IRAS 22272+5435 it is diffuse and widely developed over 2000 AU. This is at least suggestive that there is an evolutionary sequence of the hydrocarbon production in these PPNs: IRAS 05341+0852 is in the earliest stage of the evolution, followed by IRAS 04296+3429, with IRAS 22272+5435 being the most evolved in the post-AGB evolution.

Although the present sample is small, we do note that there seems to be a correlation between the size of the emitting region and the spectral evolution of the hydrocarbon emission features. The two trends in the spectral sequence, (1) the decline of aliphatic emission at 3.4 μm with respect to the aromatic emission at 3.3 μm, and (2) the decrease of the overall intensity of hydrocarbon feature integrated at 3.2–3.6 μm, apparently go together with the hydrocarbon emitting region becoming spatially more developed. It is interesting to note that a similar spectral variation of the aliphatic and aromatic hydrocarbon features has been reported in the thermal annealing of the laboratory analogs of carbon dust (Schnaiter et al. 1999; Goto et al. 2000). These results show that high spatial resolution infrared imaging spectroscopy has the capability of directly tracing the chemical evolution of circumstellar synthesis of carbonaceous compounds, with significant implications on our understanding of the chemical enrichment of the interstellar medium and the Galaxy.

REFERENCES

Clément, D., Mutschke, H., Klein, R., & Henning, Th. 2003, ApJ, 594, 642
Deguchi, S., Fujii, T., Nakashima, J., & Wood, P. R. 2002, PASJ, 54, 719
Ehrenfreund, P., & Charnley, S. B. 2000, ARA&A, 38, 427
Fujii, T., Nakada, Y., & Parthasarathy, M. 2002, A&A, 385, 884
Gaessler, W., Takami, H., Takato, N., Hayano, Y., Kamata, Y., Saint-Jacques, D., Minowa, Y., & Iye, M. 2002, Proc. SPIE, 4494, 30
Geballe, T. R. 1997, in ASP Conf. Ser. 122, From Stardust to Planetesimals, ed. Y. J. Pendleton & A. G. G. M. Tielens (San Francisco: ASP), 119
Geballe, T. R., Tielens, A. G. G. M., Kwok, S., & Hrivnak, B. J. 1992, ApJ, 387, L89
Geballe, T. R., & van der Veen, W. E. C. J. 1990, A&A, 235, L9
Goto, M., Maihara, T., Terada, H., Kaito, C., Kimura, S., & Wada, S. 2000, A&AS, 141, 149
Goto, M., et al. 2003, ApJ, 589, 419
Henning, Th., Jäger, C., & Mutschke, H. 2004, in ASP Conf. Ser. 309, Astrophysics of Dust, ed. A. N. Witt et al. (San Francisco: ASP), 603
Henning, Th., & Mutschke, H. 2001, Spectrochim. Acta, 57, 815
Henning, T., & Salama, F. 1998, Science, 282, 2204
Hrivnak, B. J., & Kwok, S. 1991, ApJ, 368, 564
Kobayashi, N., et al. 2000, Proc. SPIE, 4008, 1056
Kwok, S. 1993, ARA&A, 31, 63

Kwok, S. 2004, Nature, 430, 985
Kwok, S., Hrivnak, B. J., & Geballe, T. R. 1995, ApJ, 454, 394
Kwok, S., Volk, K., & Bernath, P. 2001, ApJ, 554, L87
Kwok, S., Volk, K. M., & Hrivnak, B. J. 1989, ApJ, 345, L51
———. 1999, A&A, 350, L35
Lord, S. D. 1992, A New Software Tool for Computing Earth's Atmosphere Transmissions of Near- and Far-Infrared Radiation (NASA Tech. Memo. 103957; Moffett Field: NASA)
Manchado, A., Garcia-Lario, P., Esteban, C., Mampaso, A., & Pottasch, S. R. 1989, A&A, 214, 139
Meixner, M., Skinner, C. J., Graham, J. R., Keto, E., Jernigan, J. G., & Arens, J. F. 1997, ApJ, 482, 897
Pendleton, Y. J., & Allamandola, L. J. 2002, ApJS, 138, 75
Sahai, R. 1999, ApJ, 524, L125
Schnaiter, M., Henning, Th., Mutschke, H., Kohn, B., Ehbrecht, M., & Huisken, F. 1999, ApJ, 519, 687
Takami, H., et al. 2004, PASJ, 56, 225
Tokunaga, A. T., et al. 1998, Proc. SPIE, 3354, 512
Ueta, T., Meixner, M., & Bobrowsky, M. 2000, ApJ, 528, 861
Ueta, T., et al. 2001, ApJ, 557, 831